www.MaterialsViews.com

ADVANCED
OPTICAL
MATERIALS
www.advopticalmat.de

COMMUNICATION

Ultrafast and Broadband Tuning of Resonant Optical Nanostructures Using Phase-Change Materials

Miquel Rudé, Vahagn Mkhitaryan, Arif Engin Cetin, Timothy Alan Miller, Albert Carrilero, Simon Wall, Francisco Javier García de Abajo, Hatice Altug, and Valerio Pruneri*

Nanophotonic devices incorporating metallic elements can support plasmons, which are collective oscillations of conduction band electrons driven by an external electromagnetic field.[1] Plasmons can confine and guide light well below the diffraction limit, and when supported by suitably engineered nanostructures, they enable the design of disruptive devices for a wide range of applications, including perfect lenses,[2] biosensors,[3] modulators,[4] plasmonic tuning,[5] and integrated waveguide circuits.[6] Plasmons also play an important role in the phenomenon of extraordinary optical transmission (EOT) of visible and infrared light through periodic arrays of subwavelength nanoholes drilled in metallic films. The observation of transmission resonances in these arrays is attributed to the resonant interaction between holes mediated by surface plasmons propagating on the film surfaces.[7] More precisely, transmission peaks emerge close to the Wood anomalies[8] and are well explained in terms of geometrical resonances in the periodic lattice.[9–11]

An important challenge in the design of plasmonic nanostructures is the precise control of their optical responses in order to meet the requirements of specific device applications. This can be accomplished by casting nanostructures with appropriate materials and geometries. However, such an approach is static and limited by material inhomogeneity and fabrication tolerances. More critically, many applications (e.g., optical switching and modulation) rely on the ability to actively change the spectral phase and amplitude of the optical response. Dynamic tuning could provide a way to reach a stable working point and at the same time modulate the

response around it. To this end, the high sensitivity of surface plasmons to local variations in the surrounding refractive index has been exploited in several approaches to achieve dynamical tuning by using active materials whose refractive index is actively changed by external stimuli. In particular, modulation of surface plasmon polaritons (SPPs) has been demonstrated using electrooptic or other effects.[4] For devices based upon EOT, liquid crystals have been used to produce controllable wavelength shifts of 10–20 nm in the near-infrared (NIR).[12] However, larger tuning ranges and faster modulation than those offered by these materials are needed for a wide range of applications.[13]

Phase-change materials (PCMs), such as $Ge_2Sb_2Te_5$ (GST), have two stable phases with very large contrast in their optical and electrical properties.[14] When PCM and metallic nanostructures supporting SPPs are properly coupled, the large changes in optical constants associated to the metal–insulator transition can be used to efficiently tune resonances. Phase transitions in PCMs can be externally driven by varying the temperature or by applying electrical or optical pulses. Importantly, these transitions can occur on the nanosecond timescale,[15,16] while the resulting phase is remarkably stable for several years.[16] Besides the widespread use of PCMs in optical storage media[14] and phase-change random access memories,[17] these properties also make them suitable for nanophotonics, where several applications have already been demonstrated.[18–21] Additionally, the capability to retain their state after a phase transition offers an opportunity to design novel reconfigurable optical elements.

In this work, we explore new designs for combining thin films of GST with arrays of nanoholes patterned in Au films and demonstrate unprecedented ultrafast and broadband optical tuning in the visible and near-infrared (vis-NIR) spectral regions of EOT devices. These coupled EOT structures provide optical resonances over a large wavelength range, while the GST permits the tuning that metals are lacking, which would not possible only using Au nanoholes. More specifically the aim of this work is twofold: first, we show large wavelength and modulation tuning of the EOT resonances based on phase (structural) transitions of GST using thermal- and current-induced effects. For properly designed geometries, shifts in the resonance wavelength as large as 385 nm—an order of magnitude higher than previously reported[12]—can be achieved. Second, we demonstrate ultrafast and large amplitude modulation of the EOT resonances in the ps regime based on changes of the resonant bond polarizability of GST.[22] Importantly, the phase-transition-induced resonance change is permanent and remains after the temperature (current) signal is switched off, while the ultrafast optical changes are completely reversible for pump powers below the threshold

M. Rudé, V. Mkhitaryan, Dr. T. A. Miller, A. Carrilero,
Prof. S. Wall, Prof. F. J. G. de Abajo, Prof. V. Pruneri
ICFO – Institut de Ciències Fotòniques
The Barcelona Institute of Science and Technology
08860 Castelldefels, Spain
E-mail: Valerio.pruneri@icfo.es
Dr. A. E. Cetin, Prof. H. Altug
Bioengineering Department
EPFL – École Polytechnique Fédérale de Lausanne
1015 Lausanne, Switzerland
Dr. A. E. Cetin
Department of Biological Engineering and Koch Institute for Integrative Cancer Research
Massachusetts Institute of Technology
Cambridge, MA 02139, USA
Prof. F. J. G. de Abajo, Prof. V. Pruneri
ICREA – Institució Catalana de Recerca i Estudis Avançats
08015 Barcelona, Spain

**ADVANCED
OPTICAL
MATERIALS**
www.advopticalmat.de

Materials Views
www.MaterialsViews.com

COMMUNICATION

Table 1. Summary of the three configurations used in this work and the different tuning mechanisms.

	D [nm]	a [nm]	GST thickness [nm]	Gold thickness [nm]	GST in holes	Thermally tuned	Electrically tuned	Optically modulated	Δλ [nm]	Resonance width
Sample A	470	250	20	40	Yes	Yes	No	Yes	385	Broad
Sample B	470	250	20	40	No	Yes	Yes	No	35	Broad
Sample C	600	200	10	125	No	Yes	No	No	13	Narrow

value that would induce phase transitions.[22] We show that the GST optical properties modify the SPPs of the Au perforated film, with the latter being essential for the existence of plasmonic resonances. The combination of temperature (current) and ultrafast-optical-pumping-induced changes thus enlarges the range of wavelength, amplitude, reversibility, and time operation in EOT-based tunable optical devices.

As summarized in **Table 1**, we study three different EOT geometries (samples A, B, and C, see below) in which we achieve a significant degree of vis-NIR optical tuning by inducing transitions of a GST layer through thermal, electrical, or optical control signals. We demonstrate spectral shifts in the resonant wavelength as large as 385 nm, combined with modulation depths of >60% associated with phase (structural) transitions by applying temperature and electrical currents. We additionally

show ultrafast subpicosecond dynamics by optical pumping, yielding >30% changes in transmission in the absence of any phase (structural) transition. The range, modulation, and speed of wavelength tuning of the investigated EOT structures are over one order of magnitude larger than those previously reported, opening new possibilities for nanophotonic devices containing PCMs, especially when one considers that electrical (thermal) and optical tuning mechanisms can be simultaneously applied.

To measure the extent to which the addition of a GST layer can alter the EOT of a patterned gold film, sample A was made. Sample A consists of a hexagonal nanohole array patterned on a 40 nm thick Au film (**Figure 1**b). A 20 nm GST film is deposited both on top of the Au film and inside the nanoholes. The device is fabricated on a fused SiO_2 substrate using colloidal lithography to create an array of
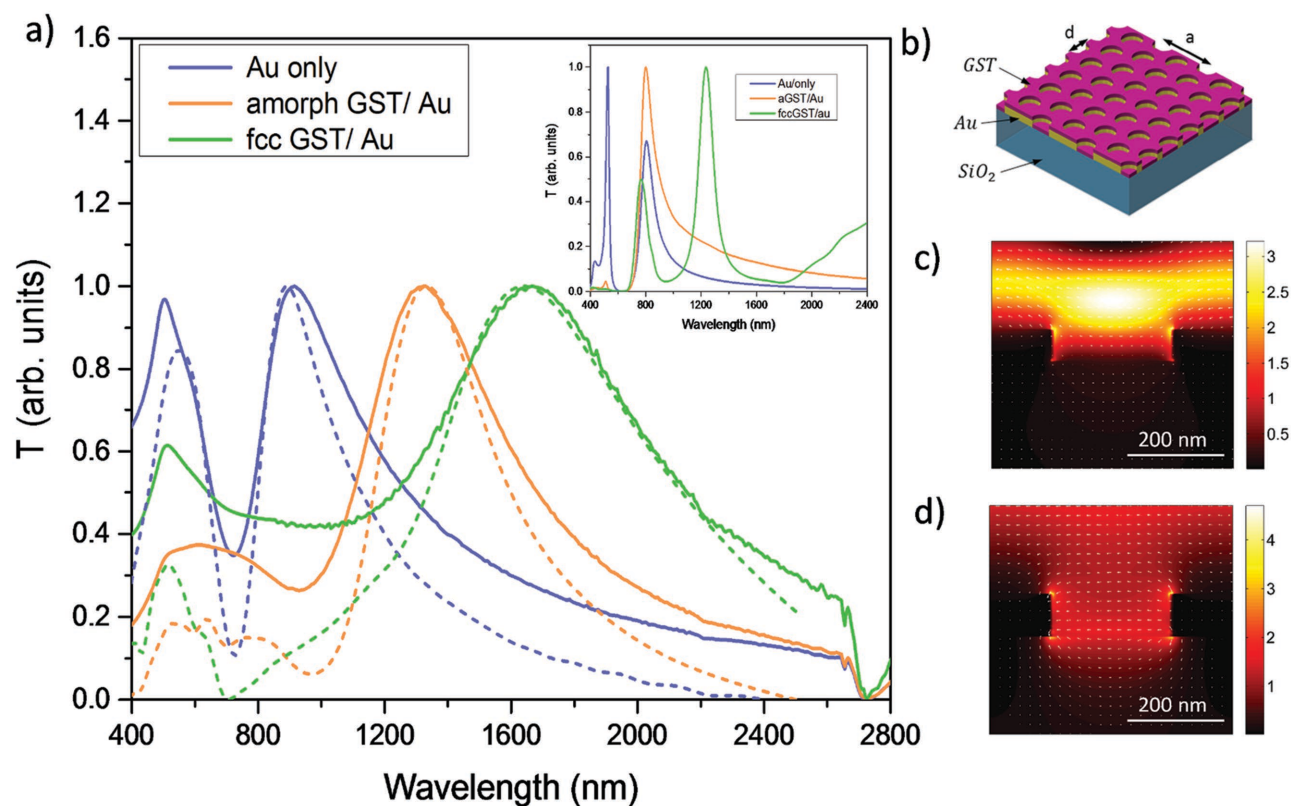
Figure 1. a) Experimental transmission (solid curves) of sample A with the GST in its amorphous (orange) and crystalline (green) phases, compared with FDTD simulations (broken curves). The transmission of a bare Au nanohole array with the same geometry is also included as a reference (blue). The actual (measured) peak transmission amplitude for the crystalline case is <40% of that for the amorphous one (this corresponds to >60% modulation depth). Inset: Corresponding calculated transmission curves based on an analytical dipole model. b) Schematic of sample A consisting of a Au nanohole array covered with a 20 nm thick GST film. Electric field distribution under c) off-resonance ($\lambda = 1200$ nm) and d) on-resonance ($\lambda = 1715$ nm) conditions when the GST is in the crystalline phase.

closely packed polystyrene beads (PS beads) with a nominal diameter of 470 nm, followed by reactive-ion etching (RIE) to shrink the diameter down to 250 nm. Finally, after 3 nm adhesive Ti layer, a 40 nm thick Au film is deposited on top using a thermal evaporator, and, after removal of the PS beads, a capping layer of 20 nm amorphous GST is deposited using radiofrequency (RF) sputtering (see the Experimental Section for details). The result is a metal film pierced by a hexagonal array (period $a = 470$ nm) of nanoholes (diameter $D = 250$ nm) and coated on top with an amorphous GST film—see scanning electron microscopy image (Figure S1b, Supporting Information).

The optical transmission spectrum for sample A is shown in Figure 1a for wavelengths in the 400–2400 nm range (see the Experimental Section). The transmission of a gold nanohole array without GST is also shown as a reference (blue curve). A peak in transmission at ≈500 nm, associated with EOT, can be clearly identified in all three cases. The transition between amorphous (orange curve) and crystalline (green curve) phases of GST is triggered by heating the sample on a hot plate at 200 °C. Shifts in the resonance wavelength (from 1330 to 1715 nm) are indicative of this phase transition in the GST film. Heating for about 1 min is sufficient to completely crystallize the film, and no further changes in the spectrum are observed after subsequent thermal treatments (see Section SI, Supporting Information). After crystallization, we observe a 385 nm redshift in the resonant wavelength, accompanied by >60% decrease in peak transmission. Figure 1c,d shows finite-difference time-domain (FDTD) simulations of the electric field distribution and optical transmission on- and off-resonance when the GST is in the crystalline phase. The simulated transmission agrees well with the experimental results, thus confirming that the large tuning is associated with significant changes in optical constants (refractive index and absorption) of the GST upon thermally driven phase (structural) transition. The calculated electric field

distribution supports the idea that the GST modifies the SPPs of the nanopatterned Au.

The same sample A was then used to investigate changes in EOT resonances via optical pumping associated with the ultrafast and reversible dynamics of resonant bond polarizability. For this purpose, a pump–probe experiment was performed (**Figure 2**a). Starting with the GST in its crystalline phase, the sample was irradiated with pump (800 nm wavelength) and probe pulses at various delay times and wavelengths. For pump fluences below the threshold required to amorphize the sample, it is known that GST is capable of transiently and rapidly acquiring values of the dielectric function close to those of the amorphous state without completing the phase transformation.[22] More importantly, this effect is ultrafast. Figure 2a shows the dynamics of Sample A during the initial 3 ps following the pump pulse. In order to make sure that the dynamics are related to the GST nanopatterning, we further repeat the same pump–probe experiment using a bare Au nanohole sample (i.e., without GST), which shows pumping the Au film does not modify the Au SPPs (no changes in transmission were observed). At telecom wavelengths around 1550 nm (Figure 2b), the combined sample shows a decrease in transmission due to the ultrafast change in the dielectric function of GST. The modulation in transmission is fast, reaching a peak value in 100 fs (resolution limited) and recovering after a few ps. Furthermore, the magnitude of the modulation is already >30% for modest excitation power.

The origin of this modulation is a transient change in the dielectric function in the ps timescale.[22] It has been shown that in this case the dielectric function achieves values which are close to, but not equal, to those of the stable amorphous phase, thus a new resonant feature arises in this regime which does not need to be the same as in the static case. This can be clearly seen for instance at $\lambda = 1550$ nm, where the change is positive in the static case and negative in the
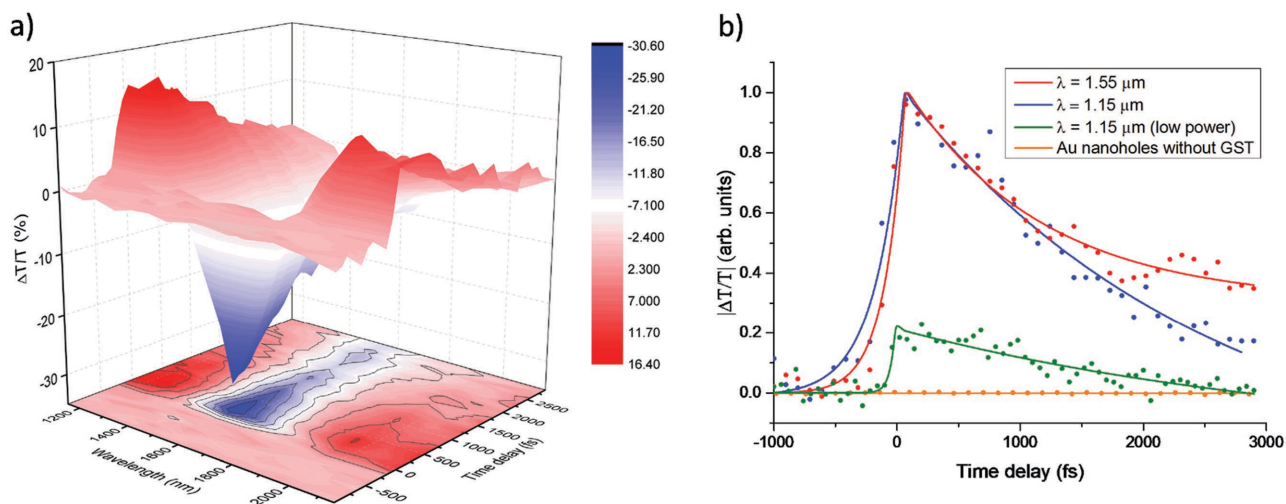
Figure 2. a) Time response of Sample A in the $\lambda = 1150$–2100 nm range during the initial 3 ps. The sample consists of an Au nanohole array covered with a 20 nm thick GST film. b) Normalized time response of the device at $\lambda = 1.15$ μm and $\lambda = 1.55$ μm using a pump fluence of $F = 5$ mJ cm^{-2}. For both wavelengths the device shows a prompt change in transmission after photoexcitation followed by an exponential recovery. At $\lambda = 1.15$ μm and lower pump fluences ($F = 1.5$ mJ cm^{-2}, green circles) the sample shows the same behavior with a smaller modulation. The time response of a device containing only a Au nanohole array without GST (orange circles) is also shown at $\lambda = 1.15$ μm.

COMMUNICATION

ultrafast regime. Without a complete characterization of the dielectric function of the sample in the IR region probed here one cannot give a definitive statement of the origin of the positive signals appearing at other wavelengths, but it most likely arises from an interference between the change in dielectric function that results from the change in resonant bonding, the change due to a transient increase in carriers induced by the pump, phonon contributions and the effects of the nanostructuring.[23]

To verify that the GST enables control of the Au SPPs, a sample was made without GST present in the patterned holes. Sample B consists of a nanohole array with the same geometry as in Sample A, but the 20 nm thick GST film is not present inside the holes and only covers the top flat Au surface (see Section SII and Figure S2, Supporting Information). This sample is also used to demonstrate electrical tuning of the combined Au EOT/GST structure. The fabrication procedure is identical to Sample A, except that the PS beads are removed after deposition of GST. In this sample, the GST amorphous-to-crystalline transition driven by heating produces a resonance wavelength blue shift ≈35 nm, while the transmission slightly decreases from 28% to 24%. These changes are in agreement with our FDTD simulations (see Section SII, Supporting Information) and confirm the reliability of modeling, which can be used in designing and optimizing future designs. We also demonstrate optical tuning of Sample B by triggering the GST transition with electrical signals. Using two lateral 40 nm thick Au films as planar contact electrodes and applying a DC current (3.5 V, 1.5 A), crystallization is achieved in 20 s due to Joule heating of the Au film underneath the GST. The results (see Section SII, Supporting Information) confirm that the electrically driven transition to a crystalline phase produces the same optical response as that obtained by direct heating.

Certain applications, such as tunable filters or optical biosensors, require narrower resonances than those achieved through the nonperfectly periodic metal arrays of samples A and B. With this purpose in mind, we investigated periodic nanohole arrays perforated in a 100 nm free-standing Si_3N_4 membrane covered with a 125 nm thick Au film and a 10 nm GST film (**Figure 3**b). The device is fabricated using a combination of deep ultraviolet lithography and RIE, as described in ref. [12]. This allows us to pattern a square lattice (period $a = 600$ nm) of nanoholes (diameter $D = 200$ nm) displaying much sharper resonances in the transmission spectrum (Sample C). Figure 3a shows the measured and simulated transmission spectra for Sample C without GST and with GST in both phases (see the Experimental Section for details). Note that the wavelength range and the resonance bandwidths are respectively about 20 times and ten times smaller than the corresponding values for Sample A. Similar to Sample B, crystallization induces a blue shift, except that the effect is now weaker (only 13 nm shift), which is consistent with the smaller thickness used for the GST layer (10 nm).

The physical origin of the large tuning observed in the experiments lies in the optical contrast of GST. After phase transition, both its refractive index and absorption coefficient increase for wavelengths above 450 nm, which lower transmission and shifts the resonant peak in the crystalline phase to either shorter or longer wavelengths, respectively, depending on whether the GST is present only on top of the Au film (samples B and C) or also inside the holes (sample A).

We gain further insight into the effect of GST phase transitions on the SPP-mediated EOT through a qualitative description based on a semianalytical model that describes the interaction of light with the nanostructured surface.[11] Because the hole diameter and array period are smaller than the wavelength, a single beam contributes to the far-field transmission, which we calculate by treating each hole as an equivalent set of dipoles. More precisely, under normal incidence, surface-parallel magnetic dipoles dominate the response, one on either side of the film (see Section SIII, Supporting Information).[11]
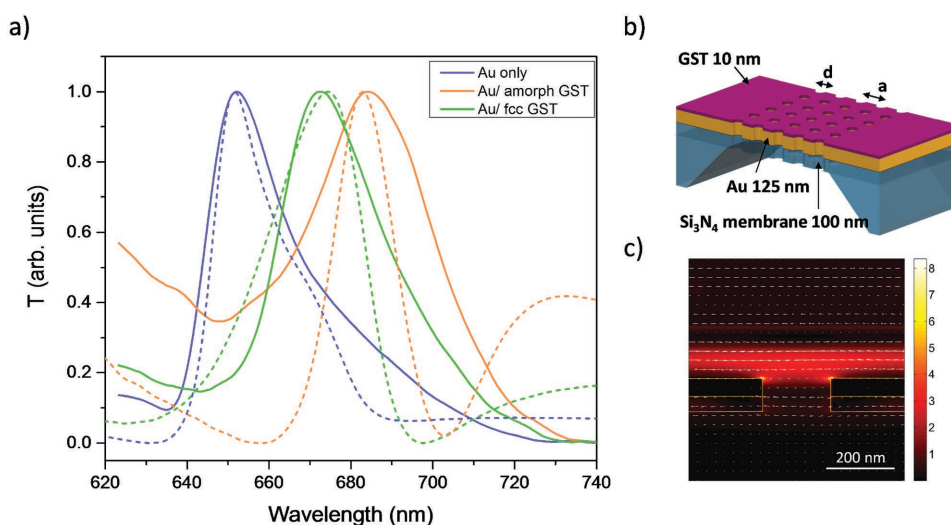
Figure 3. a) Normalized transmission (solid curves) in both the amorphous (orange) and crystalline (green) phases, compared with FDTD simulations (broken curves). Transmission of the same device without the GST film on top is also included as a reference (blue). b) Schematic of sample C consisting of a Au nanohole array suspended on a Si_3N_4 membrane with a top layer of GST (10 nm). c) Electric field distribution at the resonance wavelength of the crystalline phase ($\lambda = 670$ nm).

Then, the transmission coefficient of the array can be expressed through the induced magnetic dipole moment m_2 on the far side of the film as

$$T = \left| \frac{2\pi i k m_2}{A} (1 - r_{23}) \right|^2 \tag{1}$$

where m_2 represents the analytical expression

$$m_2 = \frac{\alpha_{M2}}{(1 - \alpha_{M1} G_1)(1 - \alpha_{M2} G_2) - \alpha'_{M1} \alpha'_{M2} \, G_1 G_2} \, H_{ext} \tag{2}$$

Here, H_{ext} is the external magnetic field at the opening of hole, including the specularly reflected field from the metal surface, a_{M1} and a_{M2} ($\alpha'_{M1} \alpha'_{M2}$) are the magnetic polarizabilities of the upper and lower sides of the hole as seen from the near (far) side, and G_1 and G_2 are the lattice sums over dipole–dipole inter-hole interactions on the near and far sides, respectively. These lattice sums display characteristic divergences which appear as lattice resonances in the spectra (see Section SIII, Supporting Information). The magnetic polarizabilities and lattice sums both depend on the surrounding environment and geometrical parameters and are therefore sensitive to the presence and optical properties of the GST material. Further details of this analytical model are offered in the Supporting Information.

Despite its simplicity, this model yields spectra (Figure 1a, inset) in qualitative agreement with experiment. In particular, it also describes large shifts in the GST-covered sample compared to bare gold. The model permits ascribing the observed resonances to the (±1,0) and (0,±1) lattice resonances, with the shift from the Wood anomaly condition (i.e., that these diffracted beams become grazing) originating in the interaction with the GST-phase-sensitive environment. The difference in magnitude and direction of the shifts between sample A (redshift) and samples B and C (blueshift) is due to the presence of GST inside the holes in sample A. The position of the resonance wavelength is given by the combined effect of the change in the polarizability of the holes (α_i) and the change in the interaction between the holes (G_i), which depends only on the material on top and the geometry. In the case of Sample A, the polarizability of the holes increases when the GST crystallizes, thus redshifting the resonance position, and this effect surpasses the small blue shift due to the change in the interaction terms. However, in samples B and C the combined effect leads to a blueshift due to a smaller change in the polarizability.

In contrast to the equilibrium regime, the ultrafast tuning is associated with changes in the resonant bond polarizability produced by photo-induced breakdown of the resonant bonds of the crystalline phase.[22] In this intermediate, nonequilibrium state, a large decrease in real and imaginary parts of the dielectric function could be observed similar to the equilibrium amorphous state. This change, in turn, leads to a change in transmission of the structure in a different way compared to the equilibrium regime discussed above.

The plasmonic nature of the observed resonances is further supported by FDTD numerical simulations (Figure 1a, broken curves), which yields spectra in excellent agreement with experiment (solid curves) and allows us to explore the near field under either off- (Figure 1c) or on-resonance (Figure 1d) conditions. The off-resonance field is mainly distributed in the near side of the film, with little penetration inside the hole. In contrast, the resonant field is strongly localized on the edges of the holes' openings and reaches higher absolute values. These results are consistent with our interpretation of plasmon-mediated lattice resonances, involving large holes' polarization at the transmission maxima.

In conclusion, we have demonstrated optical tuning of resonant nanohole array structures patterned in an Au film using the well-known phase-change material GST (**Figure 4**). The high contrast in the optical properties of GST enables thermal tuning of the resonant response with spectral shifts as large as 385 nm and modulation depths larger than 60%, well beyond those previously reported for other designs. Additionally, in one of the samples we have shown that electrical tuning can also be
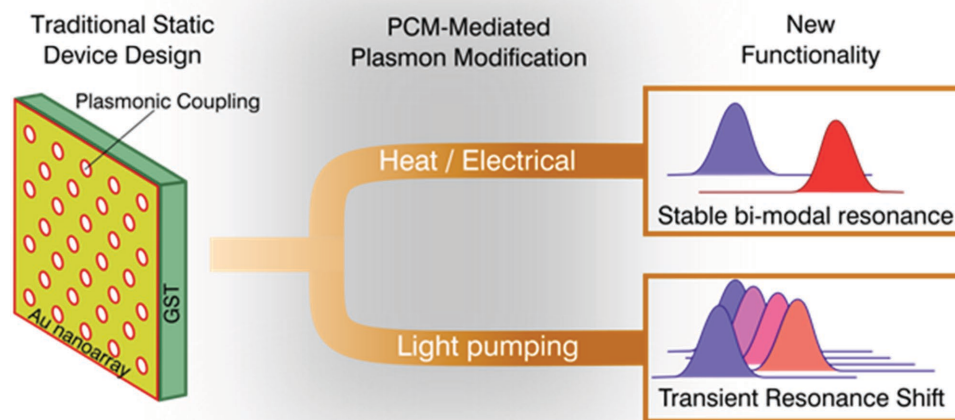
Figure 4. Summary of combined GST/EOT device control. The addition of a phase change material into traditional EOT device design greatly improves device flexibility. One retains all the control traditionally offered by static EOT device design over resonance wavelength and bandwidth. However, the inclusion of GST allows the EOT device to be controlled in all the ways that one may change GST optical properties. This allows the use of the device in a bimodal way with long-term stability, an ultrafast way with transient modification, as well as in a configuration directly compatible with existing electrooptic devices.

COMMUNICATION

achieved using Au electrodes to crystallize the GST, obtaining results similar to the thermal case. Moreover, for the sample exhibiting the largest shift and modulation, our work shows that the tuning can also be optically induced without the GST undergoing any phase transition, thus extending the device lifetime. The resulting optically induced modulation is still large (30%) in the experiments but can be improved and it occurs over an ultrafast timescale in the picosecond domain. Finally, we have also shown that this effect can be exploited in the visible regime by designing a resonant nanostructure with sharper resonances and larger Q-factors using e-beam lithography, opening a way to use them for different applications, like biosensors.

Although the GST cycleability is 10^5–10^7 cycles[16] and is limited by accumulated stress with the surrounding material due to density differences between the amorphous and crystalline phases ($\Delta\rho = 4\%$), in this case the absence of a phase transition makes it possible to continuously modulate the response on the ps timescale without any long term permanent change or damage. The ultimate repetition limit of this modulation should be given by thermal diffusion of the pump energy through the substrate before heat accumulation causes an eventual GST amorphization. This is a consideration in devices with a high degree of integration, which could be potentially optimized for heat management (e.g., by resorting to highly thermally conductive materials) to enable high repetition rates in the range of current microelectronics computation speeds. Note that the measurement presented in Figure 2 consists of more than 500 000 excitations without detectable deterioration of the optical response of the material. It is worth pointing out that the gold nanohole pattern and the GST thin films are both quite uniform despite having used scalable deposition and lithography techniques. This was confirmed by measuring the optical response while scanning the beam across the sample area, which no significant variations observed.

With proper scaling, the proposed designs, which we demonstrate in the visible and near-infrared spectral regions, can be extended to the mid-infrared, as phase change materials also exhibit large changes of optical constants at longer wavelengths. The low-cost nanofabrication methods used in this work[24,25] for patterning nanostructures incorporating phase change materials hold great potential as the basis to manufacture ultrafast and tunable optical devices operating over a wide spectral range.

Experimental Section

Fabrication of Nanohole Arrays Using Colloidal Lithography: Nanohole arrays were fabricated using colloidal lithography. 50 µL of PS beads solution (10% concentration), with a nominal diameter of 470 nm, was mixed in ethanol in a 1:1 volume ratio and placed in an ultrasonic bath for 30 min. A laminar flow of the prepared solution was then created on the surface of distilled water using a curved pipette. Water was contained in a small box where the SiO_2 substrates had been immersed previously. After a few minutes, the water surface was covered by a polycrystalline monolayer of hexagonally packed PS beads and after removing the distilled water these monolayers were deposited on top of the substrates. Shrinking of the PS beads down to 250 nm was achieved with RIE using O_2 plasma for 4:15 at 100 W. Then, a 5 nm Ti layer and a 40 nm Au layer were thermally evaporated on top. The Ti layer was used as an adhesion layer between the substrate and the Au. Finally, after (sample

A) or before (sample B) removing the PS beads using scotch tape, a 20 nm thick layer of GST was deposited by RF cosputtering from high purity targets of GeTe and Sb_2Te_3 in an Ar atmosphere (3.75 mTorr) for 90 s. X-ray diffraction of GST films prepared under the same conditions confirmed the initial phase of the material to be amorphous.

Transmission Measurements: Transmission measurements for Samples A and B were performed at normal incidence for wavelengths between 300 and 2400 nm in a commercial spectrophotometer using a 5 nm wavelength step and a rectangular beam of 3×8 mm^2.

Optical characterization of the Au nanohole arrays suspended on a Si_3N_4 membrane was performed via spectroscopic measurements, using an unpolarized broadband white light source. Transmitted light from the chip was collected by a high-magnification objective lens (100× Nikon objective lens with NA of 0.6 embedded in a Nikon Eclipse-Ti microscope) coupled with an optical fiber and recorded with a Maya 2000Pro spectrometer.

Pump–Probe Experiments: The time response of Sample A was measured using an optical pump–probe setup. 35 fs laser pulses at 800 nm with a fluence of 5 mJ cm^{-2} were used to pump the sample with a repetition rate of 80 Hz. Infrared pulses with a duration of 60 fs generated in an optical parametric amplifier measured the transmission of the sample at different time delays from 1150 to 2150 nm in 100 nm spectral steps. The transmitted light was collected using a photodiode and lock-in detection. The amplitude of the diode was recorded as a function of probe delay, generating the signal presented. The reduced repetition rate was needed to avoid both cumulative heating of the sample film by the pump pulses and melting followed by subsequent reamorphization.

[1] M. Born, E. Wolf, in *Principles of Optics: Electromagnetic Theory of Propagation, Interference and Diffraction of Light*, Cambridge University Press, Cambridge, UK **1999**.

[2] J. B. Pendry, *Phys. Rev. Lett.* **2000**, *85*, 3966.

[3] S. Lal, S. Link, N. J. Halas, *Nat. Photonics* **2007**, *1*, 641.

[4] D. Pacifici, H. J. Lezec, H. A. Atwater, *Nat. Photonics* **2007**, *1*, 402.

[5] M. A. Kats, R. Blanchard, P. Genevet, Z. Yang, M. M. Qazilbash, D. N. Basov, S. Ramanathan, F. Capasso, *Opt. Lett.* **2013**, *38*, 368.

[6] R. Charbonneau, P. Berini, E. Berolo, E. Lisicka-Shrzek, *Opt. Lett.* **2000**, *25*, 844.

[7] W. L. Barnes, W. A. Murray, J. Dintinger, E. Devaux, T. W. Ebbesen, *Phys. Rev. Lett.* **2004**, *92*, 107401.

[8] H. F. Ghaemi, T. Thio, D. E. Grupp, T. W. Ebbesen, H. J. Lezec, *Phys. Rev. B* **1998**, *58*, 6779.

[9] L. Rayleigh, *Philos. Mag.* **1907**, *14*, 60.

[10] U. Fano, *Phys. Rev.* **1936**, *50*, 573.

[11] F. J. G. de Abajo, *Rev. Mod. Phys.* **2009**, *79*, 1267.

[12] A. E. Cetin, A. Mertiri, M. Huang, S. Erramilli, H. Altug, *Adv. Opt. Mater.* **2013**, *1*, 915.

[13] A. M. Brown, M. T. Sheldon, H. A. Atwater, *ACS Photonics* **2015**, *2*, 459.

[14] M. Wuttig, N. Yamada, *Nat. Mater.* **2007**, *6*, 824.

[15] D. Loke, T. H. Lee, W. J. Wang, L. P. Shi, R. Zao, Y. C. Yeo, T. C. Chong, S. R. Elliott, *Science* **2012**, *336*, 1556.

[16] *Phase Change Materials: Science and Applications* (Eds: S. Raoux, M. Wuttig), Springer Verlag, New York **2008**.

[17] M. Wuttig, *Nat. Mater.* **2005**, *4*, 265.

[18] M. Rudé, J. Pello, J. Osmond, G. Roelkens, J. J. G. M. van der Tol, V. Pruneri, *Appl. Phys. Lett.* **2013**, *103*, 141119.

[19] C. Rios, P. Hosseini, C. D. Wright, H. Bhaskaran, W. H. P. Pernice, *Adv. Mater.* **2014**, *26*, 1372.

[20] A. K. U. Michel, P. Zalden, D. N. Chigrin, M. Wuttig, A. M. Lindenberg, T. Taubner, *ACS Photonics* **2014**, *1*, 833.

[21] P. Hosseini, C. D. Wright, H. Bhaskaran, *Nature* **2014**, *511*, 206.

[22] L. Waldecker, T. Miller, M. Rudé, R. Bertoni, J. Osmond, V. Pruneri, R. E. Simpson, R. Ernstorfer, S. Wall, *Nat. Mater.* **2015**, *14*, 991.

[23] T. Miller, M. Rudé, V. Pruneri, S. Wall **2015**, arXiv:1601.06033. arXiv.org e-Print archive. http://arxiv.org/abs/1601.06033 (accessed: April 2016).

[24] P. Patoka, M. Giersig, *J. Mater. Chem.* **2011**, *21*, 16783.

[25] S. Aksu, A. E. Cetin, R. Adato, H. Altug, *Adv. Opt. Mater.* **2013**, *1*, 798.